Open Access

This article is licensed under CC-BY-NC-ND 4.0

Article

Enhancement of Reactivity of a Ru^{IV}−Oxo Complex in Oxygen-Atom-Transfer Catalysis by Hydrogen-Bonding with Amide Moieties in the Second Coordination Sphere

Tomoya Ishizuka, Taichi Kogawa, Chisato Ogawa, Hiroaki Kotani, Yoshihito Shiota, Kazunari Yoshizawa, and Takahiko Kojima*

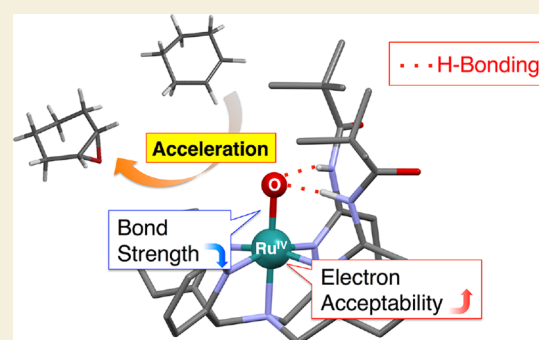Cite This: JACS Au 2023, 3, 2813−2825

Read Online

ACCESS | Metrics & More | Article Recommendations | SI Supporting Information

ABSTRACT: We have synthesized and characterized a Ru^{II}−OH$_2$ complex (**2**), which has a pentadentate ligand with two pivalamide groups as bulky hydrogen-bonding (HB) moieties in the second coordination sphere (SCS). Complex **2** exhibits a coordination equilibrium through the coordination of one of the pivalamide oxygens to the Ru center in water, affording a η^6-coordinated complex, **3**. A detailed thermodynamic analysis of the coordination equilibrium revealed that the formation of **3** from **2** is entropy-driven owing to the dissociation of the axial aqua ligand in **2**. Complex **2** was oxidized by a Ce^{IV} salt to produce the corresponding Ru^{III}(OH) complex (**5**), which was characterized crystallographically. In the crystal structure of **5**, hydrogen bonds are formed among the NH groups of the pivalamide moieties and the oxygen atom of the hydroxo ligand. Further 1e$^-$-oxidation of **5** yields the corresponding Ru^{IV}(O) complex, **6**, which has intramolecular HB of the oxo ligand with two amide N−H protons. Additionally, the Ru^{III}(OH) complex, **5**, exhibits disproportionation to the corresponding Ru^{IV}(O) complex, **6**, and a mixture of the Ru^{II} complexes, **2** and **3**, in an acidic aqueous solution. We investigated the oxidation of a phenol derivative using complex **6** as the active species and clarified the switch of the reaction mechanism from hydrogen-atom transfer at pH 2.5 to electron transfer, followed by proton transfer at pH 1.0. Additionally, the intramolecular HB in **6** exerts enhancing effects on oxygen-atom transfer reactions from **6** to alkenes such as cyclohexene and its water-soluble derivative to afford the corresponding epoxides, relative to the corresponding Ru^{IV}(O) complex (**6′**) lacking the HB moieties in the SCS.

KEYWORDS: ruthenium-oxo complex, proton-coupled electron transfer, hydrogen bonding, oxygen-atom transfer, second-coordination sphere

INTRODUCTION

Metal complexes catalyze various important and useful reactions as observed in enzymatic conversion[1−4] and industrial production.[5,6] In the catalytic reactions performed by metalloenzymes, the arrangements in the second coordination sphere (SCS) of the metal center play indispensable roles in enhancing the catalytic reactivity and improving the selectivity.[7,8] To date, a number of metal complexes bearing specific SCSs have been synthesized to exhibit unique catalytic reactivity from viewpoints of reaction efficiency and product selectivity.[9−26] For this purpose, π-conjugated substituents[9−11] or polar functional groups[12−26] have been introduced to the ligands. Those substituents enable the complexes to form π−π interaction[9−11] or hydrogen bonding (HB)[12−26] with the ligand on the metal center or with substrates of the catalytic reactions, which efficiently control the product selectivity or accelerate the catalytic reactions. For example, Karlin and co-workers have employed four kinds of tris(2-pyridylmethyl)-amine (TPA) derivatives, which have HB amino or amide substituents, as ancillary ligands for the stabilization of Cu^{II}-superoxo complexes to investigate their reactivity in hydrogen-atom abstraction (HAA) from 2,6-di-t-butyl-4-methoxy-phenol as a substrate.[14] In consequence, the Cu complex having a stronger HB substituent in the ancillary ligand showed higher reactivity in the oxidation reaction.[14]
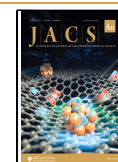
On the other hand, the impacts of HB on the oxo ligand in high-valent metal-oxo complexes have also been investigated with regard to their stability and reactivity in HAA.[16−20] For example, Borovik and co-workers synthesized a series of

Mn^{III}−oxido complexes, having urea-containing tripodal ligands with various substituents to investigate the substituent effects on the pK_a(OH) values of the Mn^{III}−hydroxo complex and also on the reactivity for HAA from organic substrates such as dihydroanthracene.[19] Both the pK_a(OH) values and rate constants for the HAA reactions correlated well with the Hammett parameters of the substituents; upon increasing the electron-withdrawing ability of the substituents, both the pK_a(OH) value and the rate constant proportionally decreased.[19] In consequence, strong HB of the urea N−Hs with the oxo ligand stabilizes the metal-oxo complexes and inevitably sacrifices the reactivity in HAA from substrates.[16−20] Since the HB decreases the basicity and electron-donating character of the oxo ligand,[19] the reactivity of high-valent metal-oxo complexes in oxygen-atom transfer (OAT) reactions should be influenced by HB (Figure 1). So far, the enhancement of the OAT reactivity by HB has yet to be demonstrated for high-valent metal-oxo complexes.[15]
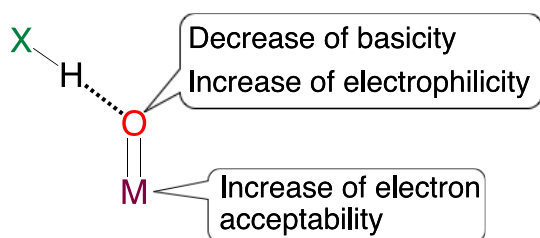

Figure 1. Effects of HB with substituents in the SCS on high-valent metal-oxo complexes.

We have investigated the reactivity of Ru^{IV}(O) complexes that have pyridylamine ligands in the oxidation of organic substrates.[27−36] The Ru^{IV}(O) complexes have been prepared by electron-transfer (ET) oxidation of the corresponding Ru^{II}−OH$_2$ complexes using a Ce^{IV} complex as an oxidant through a proton-coupled electron transfer (PCET) mechanism.[30−33] Herein, we have introduced the pivalamide group to the 6-positions of the two pyridines in pentadentate N,N-bis(2-pyridylmethyl)-N-bis(2-pyridyl)methylamine (N4Py) and synthesized a Ru^{II}−OH$_2$ complex having the pivalamide-appended N4Py ligand (DPN4Py). We have explored the coordination equilibrium observed for the Ru^{II}-DPN4Py complex owing to the coordination of one of the oxygen atoms of the two amide moieties to the Ru^{II} center; the equilibrium involves one Ru^{II} complex having DPN4Py as a hexadentate ligand and the other having it as a pentadentate ligand together with an aqua ligand. Furthermore, we have investigated the substrate oxidation ability of the corresponding Ru^{IV}(O) complex, formed by PCET oxidation of the Ru^{II}(OH$_2$) complex with a Ce^{IV} complex as an oxidant to reveal the beneficial effects of the intramolecular HB on the oxo-transfer reactivity of the Ru^{IV}(O) complex.

■ RESULTS AND DISCUSSION

Synthesis of Complex 1

According to the reported procedure, dipa (= di(2-pyridyl)-methyl-amine)[37] and BMPPA (= N-{6-(bromomethyl)pyridin-2-yl}pivalamide)[38,39] were synthesized (Scheme S1). Condensation of dipa and BMPPA in CH$_3$CN was made by the reported procedure[40] to obtain a pentadentate ligand having two pivalamide moieties, N,N-bis(6-pivalamido-2-pyridylmeth-

yl)-N-bis(2-pyridyl)methyl-amine (DPN4Py; Scheme S1). After the condensation, DPN4Py was purified from the reaction mixture by column chromatography on silica gel with a mixed solvent of ethyl acetate: MeOH = 7:3 (v/v) as an eluent. DPN4Py obtained was reacted with RuCl$_2$(DMSO)$_4$, which was prepared by a reported procedure,[41] in 2-propanol under reflux for 20 h (Scheme 1).[42] The solvent of the reaction

Scheme 1. Synthesis of Ru^{II}(DPN4Py) Complexes, 1 and 2
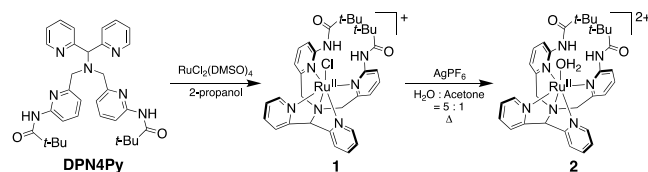
mixture was concentrated to one-fourth to precipitate a red powder, which was filtered to obtain [Ru^{II}Cl(DPN4Py)]Cl (1·Cl) in 78% yield. The counteranion of 1 was replaced by a PF$_6^-$ ion by treatment with NaPF$_6$ to obtain 1·PF$_6$.

Formation of target complex 1 was confirmed by ESI-TOF-MS spectrometry in CH$_3$CN (Figure S1); a peak cluster for 1, [Ru^{II}Cl(DPN4Py)]$^+$, was observed at m/z = 702.19 (calcd. for [Ru^{II}Cl(DPN4Py)]$^+$: m/z = 702.19). A ^{1}H NMR spectrum of 1·PF$_6$ in CDCl$_3$ at room temperature showed seven signals derived from the protons of the four pyridine rings linked to the methine or methylene carbons (Figure S2). Thus, complex 1 exhibits σ-symmetry in the solution. The assignments of the ^{1}H NMR signals were performed based on the ^{1}H−^{1}H COSY and NOE measurements. Two AX doublets with a 4H integral ratio were observed at δ 4.79 and 4.22 ppm (J_{AX} = 16.2 Hz), which were assigned to the signals of the methylene protons (Py−CH$_2$−N) of the ligand. In addition, a singlet observed at 10.9 ppm with a 2H integral ratio disappeared upon the addition of D$_2$O to the solution, and thus, this signal was assigned to the amide-NH protons bearing exchangeability. The amide-NH signal shows significant low-field shift relative to amide-NH signals in the literature (5.5−9.5 ppm)[43] and this can be explained by the strong intramolecular HB of the amide N−Hs with the axial Cl ligand even in solution.[44−46]

X-ray Diffraction Analysis of 1

Vapor diffusion of hexane as a poor solvent into a solution of 1·PF$_6$ in acetone afforded single crystals of 1·PF$_6$ suitable for X-ray diffraction analysis. The crystal structure of 1·PF$_6$ was determined, as shown in Figure 2. In the crystal of 1·PF$_6$, one ion pair of Na$^+$ and PF$_6^-$ ions per one ion pair of 1$^+$ and PF$_6^-$ ions was included, and the NaPF$_6$ salt was derived from the PF$_6^-$ source for the ion exchange during the synthesis. Both of the carbonyl oxygen atoms (O1 and O2 in Figure 2) electrostatically interact with the Na$^+$ ion with interatomic separations of 2.626(3) Å (Na⋯O1) and 2.658 Å (Na⋯O2) (Figure S4). The interatomic distances of N6⋯Cl and N7⋯Cl in the crystal structure of 1 are 3.201(3) and 3.188(3) Å (Table S1); these short interatomic distances[44,45] indicate the strong HB between the amide N−Hs and axial Cl ligand as suggested by the ^{1}H NMR spectrum (see above). Due to the HB, the bond distance of Ru−Cl (2.4336(8) Å) is longer than that of the corresponding complex having no amide moieties, [Ru^{II}Cl(N4Py)]$^+$ (Ru−Cl: 2.4162(8) Å).[42] Here, the HB between the positively polarized amide N−Hs and the Cl ligand compensates the negative charge of the Cl ligand[44,45]
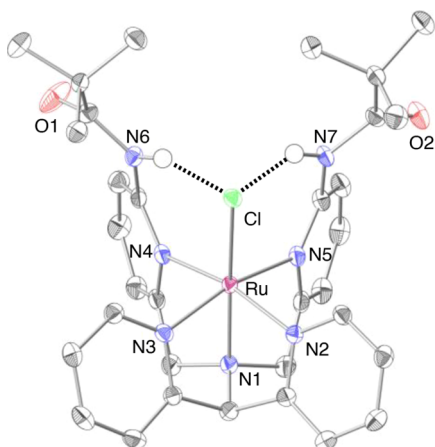
Figure 2. Crystal structure of the cationic moiety of **1**·PF₆. The thermal ellipsoids are shown at a 50% probability. The hydrogen atoms except N−Hs are omitted for clarity, and HB is expressed with dotted lines.

and thus weakens the electrostatic interaction between the Cl ligand and the Ru^{II} center to elongate the bond distance.

Synthesis of 2

The chloro complex **1**·Cl was reacted with AgPF₆ in a mixed solvent of H₂O: acetone = 5:1 v/v to obtain [Ru^{II}(DPN4Py)-(OH₂)](PF₆)₂ (**2**·2PF₆) in 39% yield.[32] Characterization of **2** was performed by elemental analysis, ESI-TOF-MS spectrometry, and ^{1}H NMR spectroscopy. In the ESI-TOF-MS spectrum of **2**, a peak-cluster was observed at m/z = 333.60, assigned to the [Ru^{II}(DPN4Py)]$^{2+}$ ion (calcd. for [Ru^{II}(DPN4Py)]$^{2+}$: m/z = 333.61) (Figure S5). Thus, the aquo ligand should be dissociated from the Ru^{II} center during the ionization.

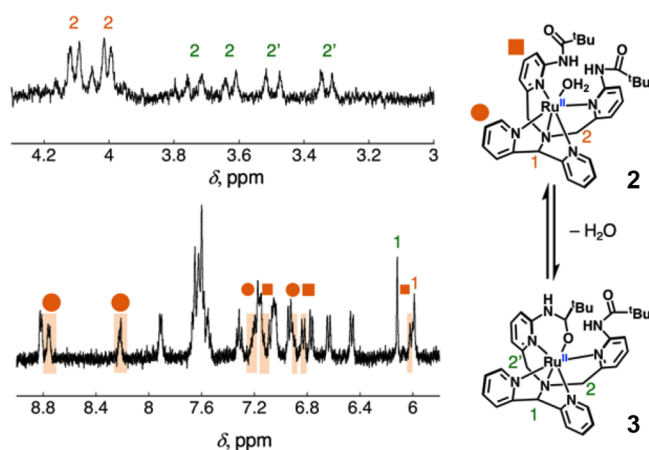The ^{1}H NMR spectrum of **2**·2PF₆ was measured at 278 K in D₂O (Figure 3). Three AB quartets derived from the

Figure 3. ^{1}H NMR spectrum of **2**·2PF₆ (0.4 mM) in D₂O (pD 2.5) at 278 K, where complexes **2** and **3** are in equilibrium. The signals derived from **2** are expressed in orange, and those of **3** are in green.

methylene protons were observed in the ^{1}H NMR spectrum of **2**, the purity of which was confirmed by elemental analysis. One AB quartet should be derived from a species having two equivalent methylene moieties (orange in Figure 3), whereas the other two AB quartets should be derived from another species having two methylene moieties that are inequivalent

with each other (green in Figure 3). The integral ratio of the AB quartets indicates that the former and latter compounds exist in a 4:6 ratio. Assignment of the ^{1}H NMR signals in the aromatic region by ^{1}H−^{1}H COSY indicates that two sets of pyridine signals are observed to be derived from the two species having inequivalent methylene C-Hs. As suggested by the crystal structure described below, the aquo ligand of **2** dissociates from the Ru center in a nonaqueous solvent and one carbonyl oxygen of the ancillary ligand occupies the vacant coordination site to afford complex **3** (see Figure 3). The ratio of **2**:**3**, the former of which has two equivalent methylene moieties and the latter has two nonequivalent ones, was determined to be 4:6 at 278 K on the basis of the integral ratio observed in the ^{1}H NMR spectrum (see above). The ^{1}H NMR spectrum of the mixture of **2** and **3** was also measured at 308 K, and the signals derived from **2** almost disappeared (Figure S6a). This change is reversible; upon lowering the temperature, the signals of **2** were recovered and the integral ratio of **2** to **3** turned back to 4:6 at 278 K. This result indicates that there is equilibrium between **2** and **3** in the aqueous medium. Thus, ^{1}H NMR spectra of **2** and **3** were measured at variable temperatures and the equilibrium constants were determined based on the ^{1}H NMR integral ratio of **2** to **3** at each temperature. And the van't Hoff plot was provided with the equilibrium constants (Figure S6b). Based on the slope and intercept of the plot, the thermodynamic parameters were determined to be $\Delta H° = 4.55 \pm 0.02$ kJ mol^{-1} and $\Delta S° = (1.3 \pm 0.1) \times 10^2$ J K^{-1} mol^{-1}. The positive enthalpy change indicates that the hexacoordinated structure of the ancillary ligand, the amide oxygen of which coordinates to the Ru^{II} center, is thermodynamically unstable in [Ru^{II}(η^6-DPN4Py)]$^+$, **3**, and the transformation from **2** to **3** is driven by the entropy gain upon releasing one H₂O molecule from the Ru^{II} center, that is, a chelate effect.

X-ray Diffraction Analyses of 3 and 4

Concentration of a solution of a mixture of **2**·2PF₆ and **3**·2PF₆ in CHCl₃ afforded yellow crystals of **3**·2PF₆, having the coordinating amide-oxygen. The crystal quality of **3**·2PF₆ was not so excellent, and the severe problems due to the crystallographic twin disturbed the explicit determination of its crystal structure. However, the coordination manner of the DPN4Py ligand in **3** was elucidated on the basis of the crystal structure (Figure S7). The number of counter PF₆ ions indicates that the total charge of **3** is +2. The carbonyl oxygen coordinating to the Ru^{II} center formed HB with the N−H group of the other amide moiety, with a N···O atomic separation of 3.04(2) Å. Unfortunately, further detailed analysis of the bond lengths and angles for **3** should be avoided due to the low crystal quality.

When NaOH aq was added to an aqueous solution of a mixture of **2** and **3** to raise the solution pH to 10, a red precipitate was formed. The red precipitate was filtered, and the obtained solid was recrystallized from CHCl₃ by solvent evaporation to afford single crystals of complex **4**·PF₆, which was the deprotonated derivative of **3** at the coordinated amide N−H moiety. An ORTEP drawing of the cationic moiety of **4**·PF₆ is shown in Figure 4. The crystal structure of **4** clarifies that one of the carbonyl oxygens of **4** coordinates to the Ru^{II} center and the total charge of **4** is +1 on the basis of the number of counter PF₆ ions. The C7−O1 bond distance for **4** (1.331(5) Å) is significantly longer than those of **3** (1.229(19) Å) and Ru^{II}-TPA complexes having O-coordinating amide
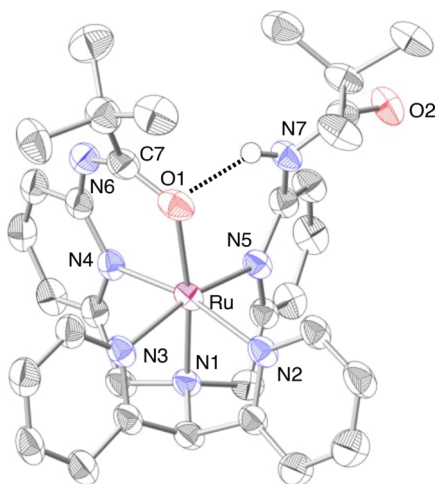
Figure 4. Crystal structure of the cationic moiety of 4·PF_6. The thermal ellipsoids are shown at 50% probability. The hydrogen atoms except N−H are omitted for clarity, and HB is expressed with a dotted line.

groups,[47−49] indicating that the amide moiety in **4**, coordinating to the Ru[II] center, is deprotonated and the anionic charge is delocalized in the amide moiety. The facile deprotonation of **3** to afford **4** can be explained by the fact that the electron density on the amide moiety is lowered by the coordination of the carbonyl oxygen to the Ru[II] center, which results in a decrease of the pK_a value of the N−H group in the amide moiety. Intramolecular HB is also formed in **4** between the carbonyl oxygen, coordinating to the Ru[II] center, and the N−H group of the other amide moiety with a N7···O1 atomic separation of 3.048(5) Å.

pK_a Determination of 3

In the Britton-Robinson buffer,[50] pH titration of **2** and **3** (50 mM) was performed by UV−vis spectroscopy (Figure S8). The absorption maxima were observed at 350 and 440 nm at pH 7.3, and upon increasing the solution pH by adding aliquots of NaOH aq (5 M), the absorption bands bathochromically shifted, and the absorption maxima appeared at 380 and 450 nm at pH 12.4 (Figure S8a). On the contrary, the absorption maxima turned back to 350 and 440 nm at pH 7.3 by adding aliquots of HCl aq (3 M) to lower the solution pH. These results demonstrate the interconversion between **4** and the mixture of **2** and **3** on the basis of the pH manipulation for the deprotonation and protonation of the coordinated amide moiety in **3** and **4** as shown in Scheme 2. When the solution pH was further decreased to 0.5, no UV−vis spectral change was observed. The absorbance changes at 380 and 450 nm plotted against the solution pH exhibited sigmoidal changes, which were analyzed to determine the pK_a values of the protonation/deprotonation of **3** to be 10.1 (Figure S8b). As mentioned above, complexes **2** and **3** are in equilibrium in the

Scheme 2. Equilibria Shown by 2 in the Aqueous Solution
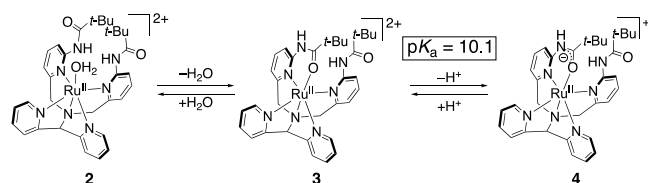
Scheme 3. PCET Oxidation of 2 and 3 in an Aqueous Solution
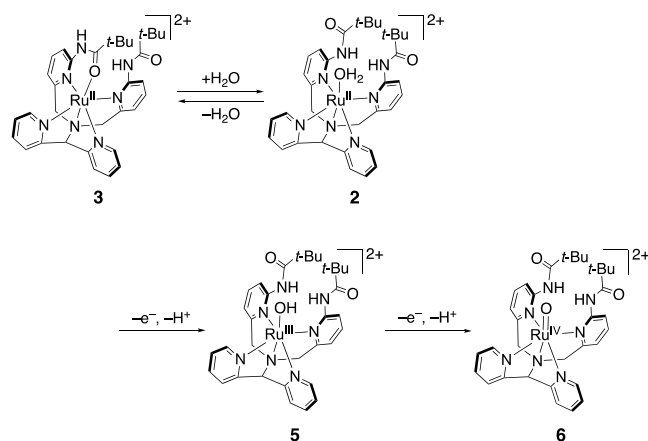
aqueous solution, and recrystallization after treatment of the solution of **2** and **3** with a strong base afforded deprotonated complex **4**. Therefore, the deprotonation showing the absorbance change should proceed at the amide N−H of **3**, coordinating to the Ru[II] center (Scheme 2).

Chemical Oxidation of a Mixture of 2 and 3

To elucidate the oxidation products of **2** and **3**, cerium(IV) ammonium nitrate (CAN) was added as an electron-transfer (ET) oxidant at 277 K to an aqueous solution of a mixture of **2** and **3**, whose pH was adjusted to 2.5 by the addition of 2% H_2SO_4 (aq), and the UV−vis spectral change was monitored (Figure 5a). The addition of CAN to the aqueous solution of **2**
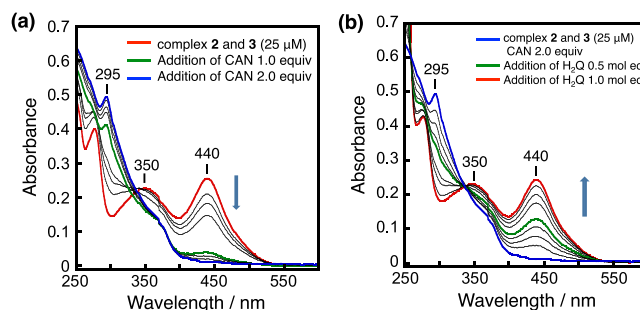

Figure 5. (a) UV−vis spectral change upon titration of **2** and **3** (25 μM) in H_2SO_4 aq (pH 2.5) with 0.25 equiv portions of CAN at 277 K: 0 equiv (red), 1 equiv (green), and 2 equiv (blue). (b) To the solution of **2** and **3** after addition of 2 equiv of CAN (blue in (a)) were added 0.5 (green) and 1.0 mol equiv (red) of hydroquinone (H_2Q) as a reductant.

and **3** caused a decrease of the metal-to-ligand charge-transfer (MLCT) bands at 350 and 440 nm. Up to the addition of 1 equiv of CAN, an isosbestic point was observed at 330 nm, and the absorbance at 440 nm, derived from the MLCT bands of **2** and **3**, almost decreased to ca. 10%. The addition of further 1 equiv CAN (2 equiv in total) afforded an isosbestic point at 370 nm and the appearance of a new absorption band at 295 nm was observed. After the addition of 2 equiv CAN, 1 mol eq of hydroquinone (H_2Q) was added as a 2e⁻ reductant to the solution to observe the recovery of the original UV−vis spectrum of **2** and **3** with 96% efficiency showing an isosbestic point at 340 nm (Figure 5b).[51,52]

ESI-TOF-MS analysis was performed for the aqueous solution of **2** and **3** after the addition of 1 equiv of CAN, followed by dilution with CH_3CN (Figure S9). In the ESI-TOF-MS spectrum, peak clusters were observed at m/z = 342.10, 719.19, and 829.19; the first one can be ascribed to $[Ru^{III}(OH)(DPN4Py)]^{2+}$ (**5**) as a dicationic product of $1e^-/1H^+$ PCET oxidation of **2**, and the second and third ones are derived from the monocationic Cl^- and PF_6^- adducts of **5**, respectively. Therefore, complex **5** should be the single product of the oxidation of a mixture of **2** and **3** through the $1e^-/1H^+$ PCET oxidation of **2**. An ESR spectrum of **5** was also measured in CH_3CN at 100 K to observe a clear ESR signal at g = 1.78, 2.21, and 2.52 (Figure S10). The ESR spectrum is typical for Ru^{III} complexes in the low-spin state (S = 1/2);[34,53,54] thus, it is confirmed that complex **5** has a Ru^{III} center.

X-ray Diffraction Analysis of 5

To an aqueous solution of **5** was added a saturated aqueous solution of KPF_6, and the mixture was kept for a week at 277 K to obtain red crystals of **5**·$2PF_6$ suitable for X-ray diffraction analysis. In the asymmetric unit of the crystal of **5**·$2PF_6$, one cation of **5** and two PF_6^- ions are included. An ORTEP drawing of **5** is shown in Figure 6. The bond length between
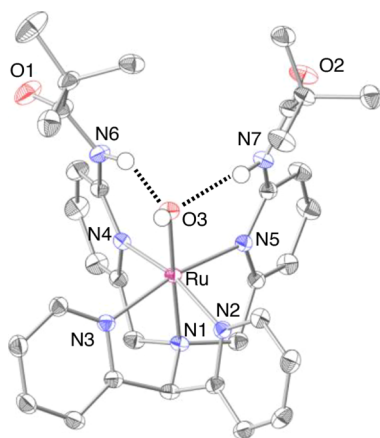

Figure 6. Crystal structure of the cationic moiety of **5**·$2PF_6$. The thermal ellipsoids are shown at 50% probability. The hydrogen atoms except N−H and O−H are omitted for clarity, and HB is expressed with dotted lines.

the Ru center and the axial oxygen atom is 1.9529(14) Å, which is significantly shorter than those of $Ru^{II}-OH_2$ complexes (2.10−2.17 Å)[32,55−58] and $Ru^{III}-OH_2$ complexes (2.03−2.18 Å)[59−61] and comparable to those of $Ru^{III}-OH$ complexes (1.95−2.01 Å).[15,62,63] Since the Ru center in **5** is in the trivalent state as evidenced by the ESR signal mentioned above, the axial ligand is not OH_2 but OH^- in light of the number of counteranions. Therefore, in the solution achieving an equilibrium between **2** and **3**, $1e^-$-oxidation with CAN exclusively proceeds on **2** to afford complex **5** through PCET oxidation, and the resultant decrease in the concentration of **2** in the solution causes the generation of **2** from **3** to maintain the equilibrium. The strongly σ-donating OH ligand in **5** causes *trans* influence and results in the elongation of the coordination bond between the Ru center and the tertiary amino nitrogen; the Ru−N1 bond lengths are 2.033(2) Å for **1**, 2.032(3) Å for **4**, and 2.0606(16) Å for **5**. Similarly to the crystal structure of **1**, the N−Hs of the amide groups in **5** also

form HB with the axial O−H ligand and the atom separations are 2.764(2) Å for N6⋯O1 and 2.807(2) Å for N7⋯O1 (Table S1).
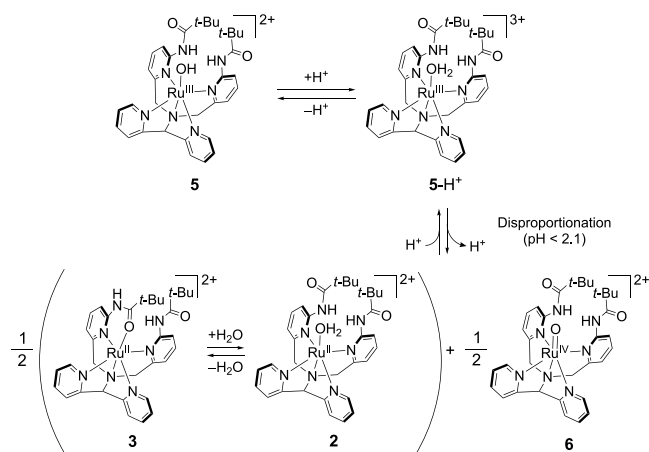
Redox Properties of 5

As mentioned above, the $Ru^{II}-OH_2$ complex, **2**, exhibits coordination equilibrium with the amide-O-coordinating derivative, **3**; thus, the proton-coupled redox properties of **2** are difficult to investigate in H_2O due to disturbance of the redox waves derived from **3**. Thus, electrochemical studies of **5** were performed instead of those of **2**. The cyclic voltammogram (CV) of **5** in H_2O at pH 2.9, containing Li_2SO_4 as an electrolyte, showed irreversible oxidation and reduction waves at +1.08 and +0.42 V vs SCE (Figure S11a). The waves can be assigned to the Ru^{IV}/Ru^{III} and Ru^{III}/Ru^{II} couples of **5** and they are irreversible, and thus the redox potential of the processes was determined by the peak potentials of the square-wave voltammogram (SWV) of **5** to be +1.08 and +0.42 V vs SCE, respectively. The anodic wave around +0.7 − +0.8 V, not observed in the first cycle but in the latter cycles, is probably derived from the Ru^{III}/Ru^{II} couple of **3**, formed around the electrode surface after the reduction of **5** to **2**. CVs and SWVs of **5** were measured at various solution pHs, and a Pourbaix diagram was provided based on the redox potentials obtained (Figure S11b). According to the Pourbaix diagram, the pK_a of the OH ligand in **5** is estimated to be 2.1, and at pH = 2.1, the Ru^{IV}/Ru^{III} couple to afford a $Ru^{IV}(O)$ complex (**6**) is changed from a $1e^-/1H^+$ process to a $1e^-/2H^+$ one. Due to the limit of the potential window under the experimental conditions, the electrochemical studies below pH < 1.5 were difficult to conduct.

To elucidate the reason why the absorbance at 440 nm was still observed upon addition of 1 equiv of CAN to an aqueous solution of **2** and **3**, the crystals of **5** (see above) were dissolved in H_2O (25 μM), whose pH was varied by addition of H_2SO_4 from 2.57 to 0.37, and the UV−vis spectra were measured at 277 K. At pH = 2.57, the absorbance at 440 nm was almost not observed (Figure S12a); however, upon lowering the solution pH below 1.5, the absorbance at 440 nm increased and, at pH 0.5, reached to ca. 25% intensity of the absorbance at 440 nm for a 25 μM solution of a mixture of **2** and **3** (Figure S12b). This can be explained by the hypothesis that the Ru^{III} complex, **5**, as a $1e^-$-oxidized product of **2** and **3** with 1 equiv CAN, undergoes disproportionation[64,65] to form **6** and a mixture of **2** and **3** at lower pH than 2 (Scheme 4). To prove the hypothesis, we have added 0.5 mol equiv of H_2Q to the aqueous solutions of **5** at pH = 2.5 and 1; both solutions exhibited the recovery of the absorbance of **2** and **3** with 99% efficiency (Figure S12c). As indicated by the Pourbaix diagram, the pK_a of the O−H ligand of **5** is estimated to be 2.1, and at a lower pH than the pK_a, complex **5** exhibits disproportionation (Scheme 4). Thus, disproportionation is probably induced by the protonation of the OH ligand to **5** to afford $[Ru^{III}(DPN4Py)(OH_2)]^{3+}$ (**5**-H^+). The protonation of the OH ligand probably destabilizes the Ru^{III} state relative to that of the mixture of the Ru^{IV} and Ru^{II} species.

Two-Electron Oxidation of 2 and 3: Formation of a Ru^{IV}−Oxo Complex

Further addition of 1 equiv of CAN to a solution of **5** affords the corresponding $Ru^{IV}(O)$ complex, **6**, as a $2e^-$-oxidized product of the mixture of **2** and **3** (Figure 5a). Complexes **5** and **6** can be reversibly reduced to the mixture of **2** and **3** (Scheme 3) by the addition of a stoichiometric amount of

Scheme 4. Disproportionation of 5 to a 1:1 Mixture of 2 and 6 Induced by Protonation of the OH Ligand

810 cm^{-1}).[27,54,66] Thus, the observed scatterings can be assigned to the stretching band of a $Ru^{IV}=O$ bond in **6**, supporting the formation of the $Ru^{IV}=O$ complex.

When 1 equiv of CAN was added to a solution of a mixture of **2** and **3** in D_2O, the ^1H NMR spectrum of the solution exhibited signals around 20 ppm, derived from a paramagnetic species (Figure S15a). The addition of 1 more equiv of CAN caused the disappearance of the signals around 20 ppm (Figure S15b) and instead showed further shifted signals in the range from 35 to −35 ppm. Further addition of one more equiv of CAN increased the intensities of the signals observed upon adding 2 equiv of CAN (Figure S15c). The ^1H NMR signals should be derived from the corresponding $Ru^{IV}(O)$ species, **6**, and the paramagnetically shifted signals indicate that the spin state of the Ru^{IV} center is $S = 1$. In contrast, the corresponding $Ru^{IV}(O)$ complex, having N4Py as the ancillary ligand, exhibited the Ru^{IV} center in the low-spin state ($S = 0$) in water.[32] The low-spin state in $[Ru^{IV}(O)(N4Py)]^{2+}$, exceptional for $Ru^{IV}(O)$ complexes,[27,31] has been explained by the extra-coordination of a water molecule to the Ru^{IV} center to form a seven-coordinate pentagonal bipyramidal structure, which can be stabilized by hydrogen bonding with water molecules;[32] however, the steric effects of the pivalamide moieties in **6** probably hinders the extra-coordination of an aqua ligand and hydrogen bonding, affording the normal six-coordinate structure of the Ru^{IV} center in the spin state of $S = 1$.

Three-Electron Oxidation of 2 and 3

Three equiv of CAN was added to an aqueous solution of **2** and **3** acidified with $HClO_4$ at pH 2.5, and after stirring for 1 h at room temperature. $NaClO_4$ and KPF_6 were added to the mixture, and the solution was kept at 278 K for 1 week to give purple crystals. Unfortunately, the crystal quality was not so high due to the crystallographic twin problems, and thus details of the crystal structure of **7** cannot be discussed.

The X-ray diffraction analysis of one of the crystals clarified that the oxidation product obtained in the crystals was a Ru^{III} complex, $[Ru^{III}(DPN4Py\text{-}O)]^{3+}$ (**7**), having a pyridine-N-oxide moiety (Scheme 5; N4 in Figure S16) formed in the DPN4Py

H_2Q. Two equiv of CAN was added to the solution of **2** and **3** in $HClO_4$ aq; then, an excess amount of KPF_6 and $NaClO_4$ was added to obtain a colorless powder of **6**. The colorless powder was dissolved in CH_3CN and analyzed by ESI-TOF-MS (Figure S13). In the ESI-TOF-MS spectrum, peak clusters appeared at m/z = 341.57 and 828.10, the former of which was assignable to the corresponding Ru^{IV}−oxo complex, $[Ru^{IV}(O)(DPN4Py)]^{2+}$ (**6**; calcd: m/z = 341.61), formed by $2e^-/2H^+$-PCET oxidation of **2** and the latter was to an ion pair of **6** with PF_6^-. When the complex was formed in $H_2^{18}O$, the peak cluster in the ESI-TOF-MS spectrum shifted to 342.58, assignable to that of $[Ru^{IV}(^{18}O)(DPN4Py)]^{2+}$ (calcd: m/z = 342.62) (Figure S14). Thus, complex **6** was formulated as $[Ru^{IV}(O)(DPN4Py)]^{2+}$.

The microscopic Raman spectra of **6**, formed by the addition of 2 equiv CAN to a solution of **2** and **3** in $H_2^{16}O$ or $H_2^{18}O$, were measured (Figure 7) upon excitation at 532 nm; a peak was observed at 798 cm^{-1} for **6** in $H_2^{16}O$ and it shifted to 756 cm^{-1} for **6** in $H_2^{18}O$. The observed isotope shift was 42 cm^{-1}, which is consistent with the corresponding calculated value of 39 cm^{-1}. Additionally, the Raman shift of **6** is in the typical range for $Ru^{IV}(O)$ complexes reported in the literature (780−

Scheme 5. Three-electron Oxidation of an Equilibrium Mixture of 2 and 3 in an Aqueous Solution to Form 7
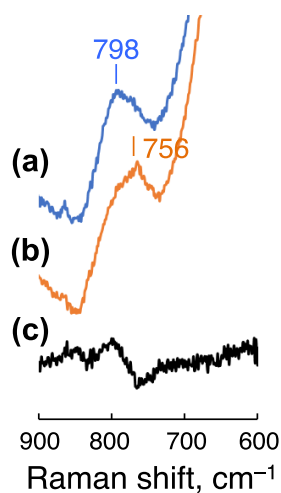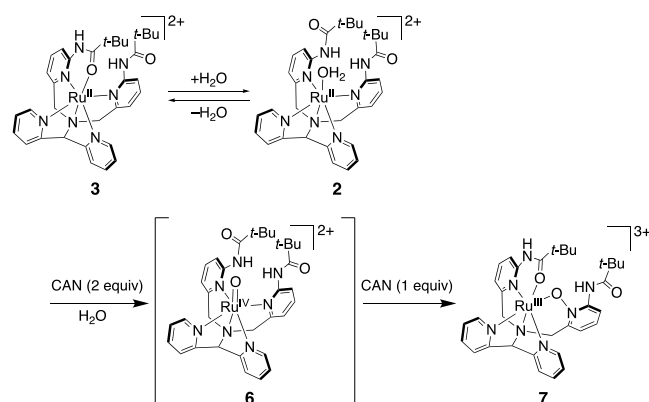

Figure 7. Microscopic Raman spectra of **6**, formed in $H_2^{16}O$ (a) and in $H_2^{18}O$ (b) and their differential spectrum ($^{16}O-^{18}O$; c). Excitation wavelength: 532 nm.

ligand, which is reminiscent of a Ru^{II} complex of a pyridine-N-oxide of TPA.[67−70] In complex **7**, one of the pyridine rings linked to a methylene carbon in the DPN4Py ligand was oxygenated to be pyridine-N-oxide and the oxygen atom of the pyridine-N-oxide moiety coordinated to the Ru^{III} center (Scheme 5). The amide oxygen of the other pyridine ring

linked to a methylene carbon also coordinated to the Ru^{III} center.

An ESI-TOF-MS spectrum was measured with a solution of the crystals of **7** in CH$_3$CN and a peak cluster was observed at m/z = 341.10 with peak separations of 0.5 (Figure S17). The peak cluster can be explained well with simulation for $\{[Ru^{III}(DPN4Py-O)]^{3+} - H^+\}^{2+}$ (m/z = 341.10). This result is supportive of the proposed structure of compound **7** in Scheme 5. In the ^{1}H NMR spectrum of an aqueous solution of **7** in D$_2$O (Figure S15d), a set of paramagnetic signals, different from those for **6** (blue squares in Figure S15b,c), was also observed (orange circles in Figure S15d). Therefore, the addition of an excess amount of CAN to the aqueous solution of **2** and **3** gradually causes overoxidation to afford the pyridine-N-oxide species, **7**, which was not observed right after the addition of an excess amount of CAN. The results suggest that complex **7** is formed via slow intramolecular OAT from the oxo ligand of **6** to the pyridine nitrogen atom to afford $[Ru^{II}(DPN4Py-O)]^{2+}$, followed by its 1e$^-$ ET oxidation by extra CAN.

Stoichiometric Oxidation of *p*-Methoxyphenol by 6

To investigate the reactivity of **6**, *p*-methoxyphenol (MP) was employed as a substrate. At first, 0.5 mol equiv of MP was added to a solution of **6**, formed with the addition of 2 equiv of CAN to a mixture of **2** and **3** in D$_2$O, whose pD was adjusted to be 1.0, and the ^{1}H NMR spectrum was measured (Figure S18). The ^{1}H NMR signals derived from MP fully disappeared, and a singlet was observed at 6.7 ppm, which can be ascribed to *p*-benzoquinone (BQ). ^{1}H NMR signals of a mixture of **2** and **3** were also observed, and the integral ratio of the ^{1}H NMR signals between (**2** + **3**) and BQ was estimated to be 2:1. Therefore, 2 molecules of **6** reacted with 1 molecule of MP to afford 1 molecule of BQ as a 4e$^-$-oxidized product exclusively (Scheme 6).[71]

Scheme 6. Oxidation of MP by 6
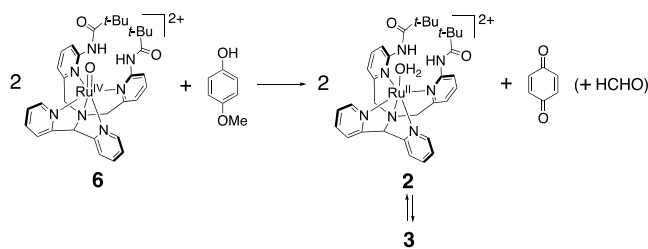
Kinetic studies on MP oxidation by **6** were performed using UV−vis spectroscopy. As can be seen in Figure 5a, under dilute conditions, complex **6** can be formed stoichiometrically by adding 2 equiv of CAN to an aqueous solution of a mixture of **2** and **3**. To an aqueous solution of **6** (25 μM), whose pH was adjusted to be 2.5 with H$_2$SO$_4$, an excess amount of MP (2.5−22 mM) was added, and the absorbance change at 440 nm was monitored (Figure S19a). The absorbance change was analyzed on the basis of pseudo-first-order kinetics to determine the apparent rate constant (k_{obs}; Table S2). The obtained k_{obs} values were plotted against the initial concentrations of MP ([MP]$_0$) and the linear relationship between k_{obs} and [MP]$_0$ was clearly observed (Figure 8a). Based on the slope of the plot, the second-order rate constant (k_2^H) was determined to be 0.98 ± 0.03 M^{-1} s^{-1} (Table 1). According to the same procedure, the k_{obs} values for the MP
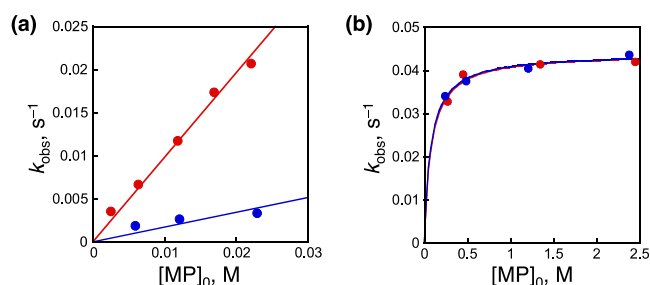
Figure 8. Plots of the apparent rate constants, k_{obs}, for the MP oxidation by **6** in H$_2$O (red circles) or D$_2$O (blue circles), whose pH or pD was adjusted to be 2.5 (a) or 1.0 (b) with H$_2$SO$_4$. The fitting curves were provided based on the second-order kinetics in (a) and on eq 1 in (b).

Table 1. Summary of Rate Constants, k or k_2, and Pre-equilibrium Constants, K, for the MP Oxidation by 6 or 6′ at 277 K

Ox	solv	pH or pD	k_2 (M^{-1} s^{-1})	k (s^{-1})	K (10^3 M^{-1})
6	H$_2$O	2.5	0.98 ± 0.03		
	D$_2$O		0.17 ± 0.03		
	H$_2$O	1.0		(4.4 ± 0.1) × 10^{-2}	12 ± 3
	D$_2$O			(4.4 ± 0.1) × 10^{-2}	13 ± 2
6′	H$_2$O	2.5		0.109 ± 0.005	2.4 ± 0.3
	D$_2$O			(3.5 ± 0.6) × 10^{-2}	2.0 ± 0.9
	H$_2$O	1.0		(8.4 ± 0.4) × 10^{-2}	3.0 ± 0.5
	D$_2$O			(2.5 ± 0.2) × 10^{-2}	2.6 ± 0.8

oxidation by **6** in D$_2$O, whose pD was adjusted to be 2.5, were also determined (Figure S19b, Table S2), and the k_{obs} was plotted against [MP]$_0$ (Figure 8a), which indicates the second-order rate constant (k_2^D) as (0.17 ± 0.03) M^{-1} s^{-1}. Thus, the kinetic isotope effect (KIE = k_2^H/k_2^D) is calculated to be 5.8. In D$_2$O, the OH group of MP should be replaced with the OD group; thus, the significant KIE indicates that the rate-determining step (RDS) for MP oxidation by **6** includes hydrogen-atom transfer (HAT) from the O−H group of MP to **6**. The influence of solution pH on the MP oxidation by **6** was investigated; in H$_2$O at pH = 1.0, the absorbance change at 440 nm for the MP oxidation by **6** was monitored and analyzed based on the pseudo-first-order kinetics to obtain the k_{obs} values (Figure S19c, Table S2). The obtained k_{obs} values were plotted against [MP]$_0$, to reveal that the k_{obs} values showed saturation behavior with increasing [MP]$_0$ (Figure 8b). This indicates that the MP oxidation by **6** at pH = 1 includes a pre-equilibrium process probably involving the adduct formation between MP and **6**. The plot of k_{obs} against [MP]$_0$ allowed us to argue the first-order kinetics including a pre-equilibrium process represented by eq 1[32] and the first-order rate constant

$$k_{obs} = kK[Sub]/(1 + K[Sub]) \qquad (1)$$

(k^H) and pre-equilibrium constant (K) was determined to be 4.4 ± 0.1 s^{-1} and (1.2 ± 0.3) × 10^4 M^{-1}, respectively. In D$_2$O at pD = 1.0, the k_{obs} values for the MP oxidation by **6** also exhibited saturation behavior against [MP]$_0$ (Figure 8b) and the k^D and K values were determined to be 4.4 ± 0.1 s^{-1} and (1.3 ± 0.2) × 10^4 M^{-1}, respectively. Thus, the KIE for MP oxidation at pH (pD) = 1.0 was calculated to be 1.0. This result indicates that the RDS of the MP oxidation at pH (pD) = 1.0 does not include the HAT from the O−H group of MP to **6** and the MP oxidation probably proceeds through ET from

MP to **6**, followed by proton transfer (PT). Supporting this assumption, the redox potential for the Ru^{IV}/Ru^{III} couple of **5** is raised from +1.08 V vs SCE at pH = 2.5 to +1.25 V (estimated)[72] at pH = 1.0 (see above). The oxidation potential of MP was determined to be +0.61 V vs SCE at pH = 2.5 and +0.69 V at pH = 1.0 in H_2O (Figure S20); thus, the driving force of the ET ($-\Delta G_{ET}$) from MP to **6** increases from 0.47 to 0.56 eV, which probably induces the switching of the reaction mechanism from HAT to ET/PT.[73−75]

To elucidate the effect of the HB moieties on the reactivity of **6**, a seven-coordinate $Ru^{IV}=O$ complex (**6′**) having N4Py as an ancillary ligand[32] was employed as the counterpart of **6** without intramolecular HB. MP oxidation by **6′** was performed at 277 K in H_2O or D_2O, whose pH or pD was adjusted to be 2.5 or 1.0 with H_2SO_4, and the reaction progress was monitored with UV−vis spectroscopy (Figure S21). According to the same procedure, the k_{obs} values were determined for the MP oxidation by **6′**, and all the k_{obs} values obtained exhibited saturation behavior against $[MP]_0$ regardless of the conditions (Figure S22); thus, the MP oxidation by **6′** includes the pre-equilibrium process based on the formation of the adduct between MP and **6′**. The k_{obs} plots against $[MP]_0$ were analyzed based on eq 1 and the obtained k and K values are summarized in Table 1. The KIE for the MP oxidation by **6′** was calculated to be 3.1 at pH = 2.5 and 3.4 at pH = 1.0. Thus, the RDS of the MP oxidation by **6′** includes the HAT from the O−H group of MP to **6′**, regardless of the solution pH. The redox potential for the Ru^{IV}/Ru^{III} couple observed for $[Ru^{II}(N4Py)(OH_2)]^{2+}$ (**2′**) is lower than that for **5** both at pH = 2.5 (+0.83 V vs SCE)[12c] and at pH = 1.0 (+0.96 V; Figure S23). Thus, the $-\Delta G_{ET}$ value from MP to **6′** is lower than 0.30 eV both at pH = 2.5 and 1.0 and the HAT reaction should be preferred to the ET/PT reaction.[76]

As described above, the MP oxidation by **6** at pH 2.5 proceeds through the HAT mechanism with second-order kinetics; however, the mechanism switches at pH = 1.0 to the ET/PT one with first-order kinetics including the pre-equilibrium process. On the other hand, the MP oxidation by the seven-coordinate **6′** without the pivalamide groups proceeds through the HAT mechanism with the first-order kinetics including the pre-equilibrium process both at pH = 2.5 and 1.0. Thus, the rate constants of the MP oxidation by **6** and **6′** cannot be directly compared. However, the k^H values for the MP oxidation by **6′** at pH = 1.0 are almost two times larger than that by **6** at the same pH (Table 1). This indicates that the HB moieties in **6** increase its electron acceptability but lower the proton acceptability of the oxo ligand; thus, the MP oxidation by **6** proceeds through the ET/PT mechanism, and the reactivity of **6** in the HAT becomes lower than **6′**, which lacks the intramolecular HB and thus maintains the strong proton acceptability of the oxo ligand.[16−20]

Catalytic Oxidation of Cyclohexene by 2

Catalytic oxidation of cyclohexene (Cy-ene) as a substrate was performed by the addition of CAN (2000 molar equiv) as a sacrificial oxidant to an aqueous solution of a mixture of **2** and **3** (1 molar equiv) and Cy-ene (1000 mol eq). A ^1H NMR spectrum of the reaction mixture after stirring for 1 min was measured, and the ^1H NMR signals of cyclohexanediol (CHD) and adipic acid (AdA) were observed as the products (Scheme 7 and Figure S25). In addition, the extracted solution from the reaction mixture with $CDCl_3$ exhibited ^1H NMR signals of adipaldehyde (Adal) (Scheme 7 and Figure S26). Thus,

## Scheme 7. Catalytic Oxidation of Cy-ene
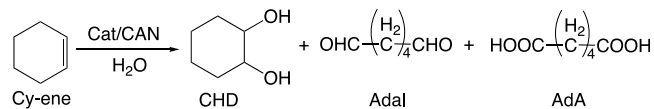
complex **6**, formed as the active species from **2** by oxidation with CAN, probably oxidizes Cy-ene through the OAT mechanism to afford cyclohexene oxide, which can be converted to CHD by hydrolysis and further to AdA by overoxidation including ring cleavage through Baeyer−Villiger-type reaction.[30] Based on the peak integration of the ^1H NMR signals, the turnover number (TON) for each product was calculated to be 215 for CHD, 100 for AdA, and 45 for Adal. CHD, Adal, and AdA are the $2e^-$, $4e^-$, and $8e^-$-oxidation products of Cy-ene, and thus, the total efficiency based on the oxidant was 58%. Only for 1 min, the total TONs for the three products reached 360, and thus, catalytic efficiency by **2** is extremely high. To compare the catalytic reactivity of **2** and **3**, we have performed catalytic oxidation of Cy-ene using $[Ru^{II}(OH_2)(N4Py)]^{2+}$, **2′**,[32] which does not have the two pivalamide groups, as a catalyst under the same conditions. As a result, the TONs catalyzed by **2′** were determined to be 90 for CHD, 75 for AdA, and 20 for Adal and the total efficiency based on the oxidant was 35%. Therefore, the catalytic activities of **2** and **3** are doubly enhanced by the introduction of the two pivalamide groups in comparison with that of **2′**. The higher TONs for **6** as the reactive species than **6′** suggest that the pivalamide groups of **6** do not exert negative steric effects on the substrate oxidation.

Kinetic Studies on Oxidation of Cyclohexene-3-Carboxylic Acid by 6

To elucidate the difference in the catalytic reactivity between the mixture (**2** and **3**) and **2′** for Cy-ene oxidation, the kinetic studies were performed on the quantitative oxidation of cyclohexene-3-carboxylic acid (CHCA), a water-soluble derivative of Cy-ene, by **6** and **6′**. To a solution of **6** (1.7 mM), which was formed by the addition of 3 mol equiv of strongly acidic CAN to a mixture of **2** and **3** in D_2O at pD = 2.5 as mentioned above, was added 10 mol equiv of CHCA as a substrate, and the reaction progress was monitored by ^1H NMR spectroscopy (Figure S27). After stirring for 1 min, the paramagnetic ^1H NMR signals derived from **6** disappeared, indicating that complex **6** was consumed by reaction with CHCA. Based on a detailed analysis of the diamagnetic region in the ^1H NMR spectrum, the product derived from CHCA was assigned to be 4-carboxy-cyclohexanediol, which should be derived from OAT from **6** to CHCA to afford the corresponding epoxide that undergoes hydrolysis under acidic conditions (Scheme 8). The yield of the diol was determined to be 83% based on the initial concentration of a mixture of **2** and **3** (Figure S28).

After adding 2 equiv of CAN to a mixture of **2** and **3** (25 μM) in H_2O at pH = 1.0 and 277 K to form $Ru^{IV}(O)$ complex

Scheme 8. Oxidation of CHCA by 6 in Acidic Water
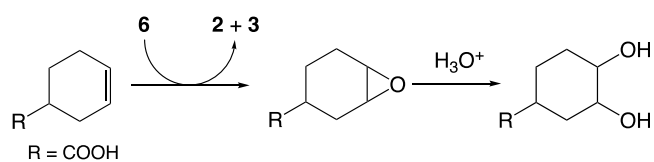
6, an excess amount of CHCA (25−51 mM) as a substrate was added to the solution of **6** to perform the substrate oxidation under pseudo-first-order conditions. The substrate oxidation was monitored by UV−vis spectroscopy; right after the addition of an excess amount of CHCA, the absorption spectrum was changed due to the difference in the solution properties by the addition of CHCA. Then, the absorbance increased at 440 nm, ascribed to **2** and **3**, in the course of the reaction, with an isosbestic point at 320 nm except for the blue line (before adding CHCA) in Figure 9a. Based on the
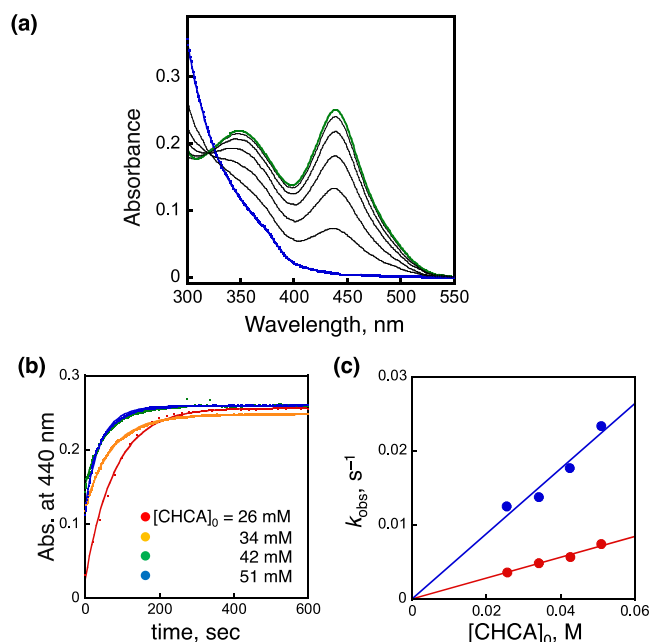

Figure 9. (a) UV−vis spectral change of a solution of **6** (25 μM), derived from **2** and **3** by addition of 2 equiv of CAN, in H_2O (pH 1.0 adjusted by H_2SO_4) upon addition of CHCA (25 mM) at 277 K. Blue line: before addition of CHCA, green line: 1200 s after addition of CHCA (25 mM). (b) Absorbance changes at 440 nm for the reaction solution of **6** with CHCA (26−51 mM) and the fitting curves based on the pseudo-first-order kinetics. (c) Dependence of the k_{obs} values for the CHCA oxidation by **6** (blue circles) and **6′** (red circles) on $[CHCA]_0$.

absorbance change at 440 nm (Figure 9b), the apparent rate constants (k_{obs}) of the CHCA oxidation were determined (Table S2). The k_{obs} values were determined by changing initial concentrations of CHCA ($[CHCA]_0$), and the linear dependence of k_{obs} on $[CHCA]_0$ was clearly demonstrated. The linear fitting of the plot of k_{obs} against $[CHCA]_0$ allowed us to determine the second-order rate constant, k_2, to be 0.44 ± 0.02 M^{-1} s^{-1} (Figure 9c). After the spectral change ceased, an excess amount of H_2Q was added as a reductant; however, no further spectral change was observed, and thus, no oxidatively active species remained in the solution. In addition, in comparison of the UV−vis spectra before and after the reaction, the absorption bands derived from complexes **2** and **3** were almost recovered, and the recovery yield was estimated to be 99% on the basis of the absorbance at 440 nm. Therefore, under the diluted conditions, complex **6** was selectively generated and completely consumed in substrate oxidation to recover complexes **2** and **3** with high efficiency.

The CHCA oxidation was also performed with **6′** as an oxidant in H_2O at pH = 1.0, and the reaction progress was

monitored with the absorbance changes at 440 nm (Figure S29). The k_{obs} values obtained from the fitting analysis of the absorbance changes also showed good linearity against $[CHCA]_0$ (Figure 9c). According to the slope of the plot of k_{obs} against $[CHCA]_0$, the k_2 value was determined to be 0.141 ± 0.003 M^{-1} s^{-1}. Therefore, the CHCA oxidation by **6** is 3 times faster than that by **6′**.

Impact of the Intramolecular Hydrogen Bonding on Oxo-Transfer Oxidation

As seen in the catalytic oxidation of Cy-ene and quantitative oxidation of CHCA, complex **6** exhibits higher reactivity in the OAT oxidation as the active species than **6′**. This can be explained by the fact that the two amide moieties form HB with the oxo ligand in **6**. The HB makes the Ru^{IV} center more electron-deficient to enhance the reactivity of the OAT to alkenes (Scheme 9). DFT-optimized structures of **6** and **6′**,

Scheme 9. Mechanism for the Enhancement of the Oxo-Transfer Reactivity of 6 by the Intramolecular HB
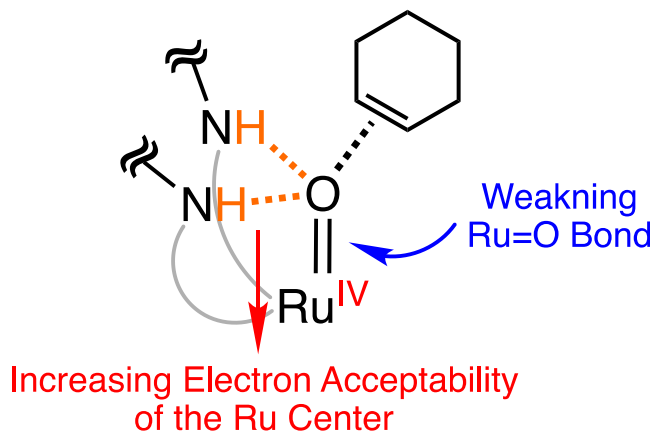
obtained from **2** and **2′** by $2e^-$ oxidation,[32] also indicate that the HB increases the positive charge on the Ru center in **6** to be +0.604028 (Figure S30), relative to that in **6′** (+0.559570; Figure S29). On the other hand, the charge on the oxo ligand in **6** is more negative, being −0.487065 in comparison with that in $[Ru^{IV}(O)(N4Py)]^{2+}$ (−0.394356). Thus, the HB in **6** enhances the polarization of the Ru═O bond, rendering the Ru^{IV} center more positive and the oxo ligand more negative. As a result of the enhanced polarization, the Ru═O bond in **6** is elongated to be 1.788 Å from 1.783 Å in **6′**. In addition, the DFT calculations indicated that the lowering of the LUMO level by the HB makes the HOMO−LUMO gap smaller and enhances the electron acceptability of the Ru center (Figure S31 and Table S3). In the case of an Fe−oxo complex with a porphyrin π-radical cation employed as the active species, an increase in the Fe−O bond length, which means that an Fe═O bond is weakened, has been reported to enhance oxo-transfer reactivity for accelerating the epoxidation of Cy-ene.[77] Therefore, the HB in **6** can accelerate the epoxidation of the olefin substrate on the basis of the enhanced electrophilicity of the Ru center and the more polarized and weakened Ru═O bond. In the literature, epoxidation of olefins by high-valent Ru−oxo complexes has been proposed to proceed through a two-step mechanism; i.e. the oxo ligand of a Ru-oxo complex attacks on one of the sp^2 carbon involved in the C═C bond of a substrate to afford a radical intermediate (the RDS), and then, the ring-closure occurs to afford the corresponding

epoxide (Scheme S2).[65,78] As seen in this mechanism, the process to afford the radical intermediate should be accelerated by the more polarized Ru—oxo complex having HB moieties. Protonation on the oxo ligand by adding a strong acid to a solution of a metal-oxo complex is also reported to promote olefin epoxidation through ET.[79,80] In this case, it has been proposed that the protonation of the oxo ligand increases the electrophilicity of the metal center and the epoxidation proceeds through ET from the olefin to the metal—oxo complex as the RDS.[79,80] Further investigation on whether the ET mechanism contributes to the epoxidation by **6** is currently underway.

CONCLUSIONS

Herein, we have synthesized a novel Ru^{II}—OH_2 complex (**2**), having an N4Py derivative (DPN4Py) functionalized with two pivalamide groups, which works as HB sites in the SCS, as the pentadentate ancillary ligand. In an aqueous solution, complex **2** exhibits an entropy-driven coordination equilibrium involving intramolecular chelation to release the aqua ligand, where the DPN4Py ligand functions as a pentadentate ligand in one component and as a hexadentate ligand including the amide-*O* coordination in the other component, **3**. Furthermore, we have revealed the redox properties of **2** in H_2O and the corresponding Ru^{III}—OH complex, **5**, was isolated through PCET oxidation of **2** and structurally characterized to establish the intramolecular HB among the amide N—H protons and the hydroxo ligand. Further $1e^-$-oxidation of **5** affords the corresponding Ru^{IV}—oxo complex, **6**, which has been characterized spectroscopically, having intramolecular HB among two amide N—H moieties and the oxo ligand, as suggested by DFT calculations. One-electron oxidation of complex **6** induces slow intramolecular OAT to generate Ru^{III} complex **7** having an O-bound pyridine-*N*-oxide derivative as a ligand. Complex **6** can oxidize *p*-methoxyphenol to *p*-benzoquinone through the HAT mechanism at pH = 2.5, whereas it can oxidize through the ET/PT mechanism at pH = 1. Additionally, catalytic oxidation of cyclohexene using **2** as a catalyst, which afforded complex **6** as the active species under the conditions, was performed to observe the superior catalytic reactivity of **2** to that of a Ru^{II}—OH_2 complex with N4Py, **2′**, as the corresponding non-HB counterpart. Complex **6** can also perform intermolecular OAT to alkenes such as Cy-ene and a water-soluble Cy-ene derivative, CHCA, under pseudo-first-order conditions. The second-order rate constant, k_2, for the CHCA oxidation by **6** is three times larger than that by **6′** of the corresponding Ru^{IV}=O complex without intramolecular HB involving the oxo ligand. Therefore, the intramolecular HB by the amide substituents with the oxo ligand on the metal center remarkably increases the oxo-transfer reactivity.

METHODS

Chemicals and solvents were used as received from Tokyo Chemical Industry (TCI) Co., Fujifilm Wako Chemicals, Nacalai Tesque, or Sigma-Aldrich Corp., unless otherwise mentioned. 2-propanol (IPA) was purchased from Fujifilm Wako Chemicals in the superdehydrated grade. Acetonitrile was distilled over CaH_2 under Ar prior to use. THF was distilled over benzophenone and sodium under Ar prior to use. Carbon tetrachloride and 2-propanol were distilled over CaH_2 under Ar prior to use.

^1H NMR measurements were performed on Bruker AVANCE 400 and 600 spectrometers. $CDCl_3$ was purified by passing it through alumina just before ^1H NMR measurements. UV—vis absorption spectra were measured on JASCO V-630 and V-780 spectropho-

tometers at 277 K, adjusted by a Peltier cooling system. ESI-TOF-MS spectra were measured on a JEOL JMS-T100CS spectrometer. Cyclic, differential-pulse, and square-wave voltammograms (CV, DPV, SWV, respectively) were recorded on a BAS Electrochemical Analyzer Model 660A. Microscopic Raman spectra were measured on a JASCO NRS-5100 spectrometer at room temperature.

ASSOCIATED CONTENT

Supporting Information

The Supporting Information is available free of charge at https://pubs.acs.org/doi/10.1021/jacsau.3c00377.

> Synthetic details, ^1H NMR, UV—vis, and ESI-TOF-MS spectra, voltammograms, UV—vis spectral changes for pK_a determination, and crystal structures and DFT-optimized structures (PDF)

AUTHOR INFORMATION

Corresponding Author

Takahiko Kojima — *Department of Chemistry, Faculty of Pure and Applied Sciences, University of Tsukuba, Tsukuba, Ibaraki 305-8571, Japan;* orcid.org/0000-0001-9941-8375; Email: kojima@chem.tsukuba.ac.jp

Authors

Tomoya Ishizuka — *Department of Chemistry, Faculty of Pure and Applied Sciences, University of Tsukuba, Tsukuba, Ibaraki 305-8571, Japan;* orcid.org/0000-0002-3897-026X

Taichi Kogawa — *Department of Chemistry, Faculty of Pure and Applied Sciences, University of Tsukuba, Tsukuba, Ibaraki 305-8571, Japan*

Chisato Ogawa — *Department of Chemistry, Faculty of Pure and Applied Sciences, University of Tsukuba, Tsukuba, Ibaraki 305-8571, Japan*

Hiroaki Kotani — *Department of Chemistry, Faculty of Pure and Applied Sciences, University of Tsukuba, Tsukuba, Ibaraki 305-8571, Japan;* orcid.org/0000-0001-7737-026X

Yoshihito Shiota — *Institute for Materials Chemistry and Engineering, Kyushu University, Fukuoka 819-0395, Japan;* orcid.org/0000-0003-2054-9845

Kazunari Yoshizawa — *Institute for Materials Chemistry and Engineering, Kyushu University, Fukuoka 819-0395, Japan;* orcid.org/0000-0002-6279-9722

Complete contact information is available at:
https://pubs.acs.org/10.1021/jacsau.3c00377

Notes

The authors declare no competing financial interest.

■ REFERENCES

(1) Bertini, I.; Gray, H. B.; Stiefel, E. I.; Valentine, J. S. *Biological Inorganic Chemistry*; University Science: Mill Valley, CA, 2007.

(2) Wikström, M.; Krab, K.; Sharma, V. Oxygen Activation and Energy Conservation by Cytochrome *c* Oxidase. *Chem. Rev.* **2018**, *118*, 2469−2490.

(3) Hoffman, B. M.; Lukoyanov, D.; Yang, Z.-Y.; Dean, D. R.; Seefeldt, L. C. Mechanism of Nitrogen Fixation by Nitrogenase: The Next Stage. *Chem. Rev.* **2014**, *114*, 4041−4062.

(4) Solomon, E. I.; Brunold, T. C.; Davis, M. I.; Kemsley, J. N.; Lee, S.-K.; Lehnert, N.; Neese, F.; Skulan, A. J.; Yang, Y.-S.; Zhou, J. Geometric and Electronic Structure/Function Correlations in Non-Heme Iron Enzymes. *Chem. Rev.* **2000**, *100*, 235−349.

(5) Appel, A. M.; Bercaw, J. E.; Bocarsly, A. B.; Dobbek, H.; DuBois, D. L.; Dupuis, M.; Ferry, J. G.; Fujita, E.; Hille, R.; Kenis, P. J. A.; Kerfeld, C. A.; Morris, R. H.; Peden, C. H. F.; Portis, A. R.; Ragsdale, S. W.; Rauchfuss, T. B.; Reek, J. N. H.; Seefeldt, L. C.; Thauer, R. K.; Waldrop, G. L. Frontiers, Opportunities, and Challenges in Biochemical and Chemical Catalysis of CO₂ Fixation. *Chem. Rev.* **2013**, *113*, 6621−6658.

(6) Makio, H.; Terao, H.; Iwashita, A.; Fujita, T. FI Catalysts for Olefin Polymerization—A Comprehensive Treatment. *Chem. Rev.* **2011**, *111*, 2363−2449.

(7) Borovik, A. S. Role of Metal-Oxo Complexes in the Cleavage of C-H Bonds. *Chem. Soc. Rev.* **2011**, *40*, 1870−1874.

(8) Zhao, M.; Wang, H.-B.; Ji, L.-N.; Mao, Z.-W. Insights into Metalloenzyme Microenvironments: Biomimetic Metal Complexes with a Functional Second Coordination Sphere. *Chem. Soc. Rev.* **2013**, *42*, 8360−8375.

(9) Yanagisawa, S.; Crowley, P. B.; Firbank, S. J.; Lawler, A. T.; Hunter, D. M.; McFarlane, W.; Li, C.; Kohzuma, T.; Banfield, M. J.; Dennison, C. π-Interaction Tuning of the Active Site Properties of Metalloproteins. *J. Am. Chem. Soc.* **2008**, *130*, 15420−15428.

(10) Meunier, A.; Singleton, M. L.; Kauffmann, B.; Granier, T.; Lautrette, G.; Ferrand, Y.; Huc, I. Aromatic Foldamers as Scaffolds for Metal Second Coordination Sphere Design. *Chem. Sci.* **2020**, *11*, 12178−12186.

(11) Fujisaki, H.; Ishizuka, T.; Kotani, H.; Shiota, Y.; Yoshizawa, K.; Kojima, T. Selective Methane Oxidation by Molecular Iron Catalysts in Aqueous Medium. *Nature* **2023**, *616*, 476−481.

(12) Xie, J.; Yikilmaz, E.; Miller, A.-F.; Brunold, T. C. Second-Sphere Contributions to Substrate-Analogue Binding in Iron(III) Superoxide Dismutase. *J. Am. Chem. Soc.* **2002**, *124*, 3769−3774.

(13) Kinzie, S. D.; Thevis, M.; Ngo, K.; Whitelegge, J.; Loo, J. A.; Abu-Omar, M. M. Posttranslational Hydroxylation of Human Phenylalanine Hydroxylase Is a Novel Example of Enzyme Self-Repair within the Second Coordination Sphere of Catalytic Iron. *J. Am. Chem. Soc.* **2003**, *125*, 4710−4711.

(14) Bhadra, M.; Lee, J. Y. C.; Cowley, R. E.; Kim, S.; Siegler, M. A.; Solomon, E. I.; Karlin, K. D. Intramolecular Hydrogen Bonding Enhances Stability and Reactivity of Mononuclear Cupric Superoxide Complexes. *J. Am. Chem. Soc.* **2018**, *140*, 9042−9045.

(15) Jitsukawa, K.; Oka, Y.; Yamaguchi, S.; Masuda, H. Preparation, Structure Characterization, and Oxidation Activity of Ruthenium Complexes with Tripodal Ligands Bearing Noncovalent Interaction Sites. *Inorg. Chem.* **2004**, *43*, 8119−8129.

(16) Cook, S. A.; Borovik, A. S. Molecular Designs for Controlling the Local Environments around Metal Ions. *Acc. Chem. Res.* **2015**, *48*, 2407−2414.

(17) Lacy, D. C.; Gupta, R.; Stone, K. L.; Greaves, J.; Ziller, J. W.; Hendrich, M. P.; Borovik, A. S. Formation, Structure, and EPR Detection of a High Spin Feᴵⱽ-Oxo Species Derived from Either an Feᴵᴵᴵ-Oxo or Feᴵᴵᴵ-OH Complex. *J. Am. Chem. Soc.* **2010**, *132*, 12188−12190.

(18) Gupta, R.; Lacy, D. C.; Bominaar, E. L.; Borovik, A. S.; Hendrich, M. P. Electron Paramagnetic Resonance and Mössbauer Spectroscopy and Density Functional Theory Analysis of a High-Spin Feᴵⱽ-Oxo Complex. *J. Am. Chem. Soc.* **2012**, *134*, 9775−9784.

(19) Barman, S. K.; Jones, J. R.; Sun, C.; Hill, E. A.; Ziller, J. W.; Borovik, A. S. Regulating the Basicity of Metal-Oxido Complexes with a Single Hydrogen Bond and Its Effect on C-H Bond Cleavage. *J. Am. Chem. Soc.* **2019**, *141*, 11142−11150.

(20) Oswald, V. F.; Lee, J. L.; Biswas, S.; Weitz, A. C.; Mittra, K.; Fan, R.; Li, J.; Zhao, J.; Hu, M. Y.; Alp, E. E.; Bominaar, E. L.; Guo, Y.; Green, M. T.; Hendrich, M. P.; Borovik, A. S. Effects of Noncovalent Interactions on High-Spin Fe(IV)-Oxido Complexes. *J. Am. Chem. Soc.* **2020**, *142*, 11804−11817.

(21) Helm, M. L.; Stewart, M. P.; Bullock, R. M.; DuBois, M. R.; DuBois, D. L. A Synthetic Nickel Electrocatalyst with a Turnover Frequency Above 100,000 s⁻¹ for H₂ Production. *Science* **2011**, *333*, 863−866.

(22) Liu, T.; DuBois, D. L.; Bullock, R. M. An Iron Complex with Pendant Amines as a Molecular Electrocatalyst for Oxidation of Hydrogen. *Nat. Chem.* **2013**, *5*, 228−233.

(23) Liu, T.; Chen, S.; O'Hagan, M. J.; DuBois, M. R.; Bullock, R. M.; DuBois, D. L. Synthesis, Characterization, and Reactivity of Fe Complexes Containing Cyclic Diazadiphosphine Ligands: The Role of the Pendant Base in Heterolytic Cleavage of H₂. *J. Am. Chem. Soc.* **2012**, *134*, 6257−6272.

(24) Han, Z.; Horak, K. T.; Lee, H. B.; Agapie, T. Tetranuclear Manganese Models of the OEC Displaying Hydrogen Bonding Interactions: Application to Electrocatalytic Water Oxidation to Hydrogen Peroxide. *J. Am. Chem. Soc.* **2017**, *139*, 9108−9111.

(25) Hong, S.; Lee, Y.-M.; Sankaralingam, M.; Vardhaman, A. K.; Park, Y. J.; Cho, K.-B.; Ogura, T.; Sarangi, R.; Fukuzumi, S.; Nam, W. A Manganese(V)-Oxo Complex: Synthesis by Dioxygen Activation and Enhancement of Its Oxidizing Power by Binding Scandium Ion. *J. Am. Chem. Soc.* **2016**, *138*, 8523−8532.

(26) Vereshchuk, N.; Matheu, R.; Benet-Buchholz, J.; Pipelier, M.; Lebreton, J.; Dubreuil, D.; Tessier, A.; Gimbert-Suriñach, C.; Ertem, M. Z.; Llobet, A. Second Coordination Sphere Effects in an Evolved Ru Complex Based on Highly Adaptable Ligand Results in Rapid Water Oxidation Catalysis. *J. Am. Chem. Soc.* **2020**, *142*, 5068−5077.

(27) Ishizuka, T.; Kotani, H.; Kojima, T. Characteristics and Reactivity of Ruthenium-Oxo Complexes. *Dalton Trans.* **2016**, *45*, 16727−16750.

(28) Kojima, T. Development of Functionality of Metal Complexes Based on Proton-Coupled Electron Transfer. *Dalton Trans.* **2020**, *49*, 7284−7293.

(29) Kojima, T. Study on Proton-Coupled Electron Transfer in Transition Metal Complexes. *Bull. Chem. Soc. Jpn.* **2020**, *93*, 1571−1582.

(30) Hirai, Y.; Kojima, T.; Mizutani, Y.; Shiota, Y.; Yoshizawa, K.; Fukuzumi, S. Ruthenium-Catalyzed Selective and Efficient Oxygenation of Hydrocarbons with Water as an Oxygen Source. *Angew. Chem., Int. Ed.* **2008**, *47*, 5772−5776.

(31) Kojima, T.; Hirai, Y.; Ishizuka, T.; Shiota, Y.; Yoshizawa, K.; Ikemura, K.; Ogura, T.; Fukuzumi, S. A Low-Spin Ruthenium(IV)-Oxo Complex: Does the Spin State Have an Impact on the Reactivity? *Angew. Chem., Int. Ed.* **2010**, *49*, 8449−8453.

(32) Ohzu, S.; Ishizuka, T.; Hirai, Y.; Jiang, H.; Sakaguchi, M.; Ogura, T.; Fukuzumi, S.; Kojima, T. Mechanistic Insights into Catalytic Oxidations of Organic Compounds by Ruthenium(IV)-Oxo Complexes with Pyridylamine Ligands. *Chem. Sci.* **2012**, *3*, 3421−3431.

(33) Ishizuka, T.; Ohzu, S.; Kotani, H.; Shiota, Y.; Yoshizawa, K.; Kojima, T. Hydrogen Atom Abstraction Reactions Independent of C-H Bond Dissociation Energies of Organic Substrates in Water: Significance of Oxidant-Substrate Adduct Formation. *Chem. Sci.* **2014**, *5*, 1429−1436.

(34) Kotani, H.; Shimomura, H.; Horimoto, M.; Ishizuka, T.; Shiota, Y.; Yoshizawa, K.; Yanagisawa, S.; Kawahara-Nakagawa, Y.; Kubo, M.; Kojima, T. Fundamental Electron-Transfer and Proton-Coupled Electron-Transfer Properties of Ru(IV)-oxo Complexes. *Dalton Trans.* **2019**, *48*, 13154−13161.

(35) Kotani, H.; Shimomura, H.; Ikeda, K.; Ishizuka, T.; Shiota, Y.; Yoshizawa, K.; Kojima, T. Mechanistic Insight into Concerted

Proton-Electron Transfer of a Ru(IV)-Oxo Complex: A Possible Oxidative Asynchronicity. *J. Am. Chem. Soc.* **2020**, *142*, 16982−16989.

(36) Ohzu, S.; Ishizuka, T.; Hirai, Y.; Fukuzumi, S.; Kojima, T. Photocatalytic Oxidation of Organic Compounds in Water by Ruthenium(II)-Pyridylamine Complexes as Catalysts with High Efficiency and Selectivity. *Chem.−Eur. J.* **2013**, *19*, 1563−1567.

(37) Lubben, M.; Meetsma, A.; Wilkinson, E. C.; Feringa, B.; Que, L., Jr. Nonheme Iron Centers in Oxygen Activation: Characterization of an Iron(III) Hydroperoxide Intermediate. *Angew. Chem., Int. Ed. Engl.* **1995**, *34*, 1512−1514.

(38) Jitsukawa, K.; Masuda, H.; Einaga, H. Synthesis and Structure of a New Tripodal Polypyridine Copper(II) Complex That Enables to Recognize a Small Molecule. *Chem. Lett.* **1995**, *24*, 61−62.

(39) Liu, P.; Chen, Y.; Deng, J.; Tu, Y. An Efficient Method for the Preparation of Benzylic Bromides. *Synthesis* **2001**, *2001*, 2078−2080.

(40) Soo, H. S.; Komor, A. C.; Iavarone, A. T.; Chang, C. J. A Hydrogen-Bond Facilitated Cycle for Oxygen Reduction by an Acid- and Base-Compatible Iron Platform. *Inorg. Chem.* **2009**, *48*, 10024−10035.

(41) Dulière, E.; Devillers, M.; Brynaert, J. M. Novel Phosphinite-Ruthenium(II) Complexes Covalently Bound on Silica: Synthesis, Characterization, and Catalytic Behavior versus Oxidation Reactions of Alcohols into Aldehydes. *Organometallics* **2003**, *22*, 804−811.

(42) Kojima, T.; Weber, D. M.; Choma, C. T. {*N*-[Bis(2-pyridyl)methyl]-*N*,*N*-bis-(2-pyridylmethyl)-amine-$\kappa^5 N$}chloro-Ruthenium(II) Perchlorate Methanol Solvate. *Acta Crystallogr., Sect. E: Struct. Rep. Online* **2005**, *61*, m226−m228.

(43) Hesse, M.; Meier, H.; Zeeh, B. *Spectroscopic Methods in Organic Chemistry*; 2nd ed.; Georg Thieme Verlag: Stuttgart, 2008.

(44) Jeffrey, G. A. *An Introduction to Hydrogen Bonding*; University Press: New York, 1997.

(45) Desiraju, G. R.; Steiner, T. *The Weak Hydrogen Bond*; Oxford Science: New York, 1999.

(46) Electrochemical studies of **1** were also performed in acetone containing $(n$-Bu$)_4$N·PF$_6$ (0.1 M) as an electrolyte (Figure S3).

(47) Kojima, T.; Hayashi, K.; Matsuda, Y. Structures and Properties of Ruthenium(II) Complexes of Pyridylamine Ligands with Oxygen-Bound Amide Moieties: Regulation of Structures and Proton-Coupled Electron Transfer. *Inorg. Chem.* **2004**, *43*, 6793−6804.

(48) Kojima, T.; Noguchi, D.; Nakayama, T.; Inagaki, Y.; Shiota, Y.; Yoshizawa, K.; Ohkubo, K.; Fukuzumi, S. Synthesis and Characterization of Novel Ferrocene-Containing Pyridylamine Ligands and Their Ruthenium(II) Complexes: Electronic Communication through Hydrogen-Bonded Amide Linkage. *Inorg. Chem.* **2008**, *47*, 886−895.

(49) Kojima, T.; Hirasa, N.; Noguchi, D.; Ishizuka, T.; Miyazaki, S.; Shiota, Y.; Yoshizawa, K.; Fukuzumi, S. Synthesis and Characterization of Ruthenium(II)−Pyridylamine Complexes with Catechol Pendants as Metal Binding Sites. *Inorg. Chem.* **2010**, *49*, 3737−3745.

(50) Britton, H. T. K.; Robinson, R. A. CXCVIII.—Universal Buffer Solutions and the Dissociation Constant of Veronal. *J. Chem. Soc.* **1931**, 1456−1462.

(51) The absorption observed below 260 nm in Figure 5b was derived from that of 1,4-benzoquinone, formed by the oxidation of hydroquinone.

(52) After addition of 0.5 mol eq of H$_2$Q, absorbance at 440 nm, derived from the MLCT band of **2** and **3**, recovered to *ca.* 50% relative to that expected for 25 μM mixture of **2** and **3**. This indicates that the reduction of 2e⁻-oxidized species of **2** and 3, i.e. complex **6**, with H$_2$Q directly affords the corresponding Ru^{II} complex, **2** and **3**, without apparent formation of the Ru^{III} complex, **5**.

(53) Schneider, R.; Weyhermüller, T.; Wieghardt, K. Mononuclear and Dinuclear Ruthenium Complexes Containing the LRu(acac) Fragment. Crystal Structures of [LRu^{III}(acac)(OH)]PF$_6$·H$_2$O, [{LRu^{III}-(acac)}$_2$(μ-O$_2$H$_3$)](PF$_6$)$_3$, and [{LRu^{III}(acac)}$_2$(μ-O)]-(PF$_6$)$_2$. Characterization of the Mixed-Valence Species [lLRu-(acac)}$_2$(μ-O)](PF$_6$)$_3$ (L = 1,4,7-Trimethyl-1,4,7-triazacyclononane). *Inorg. Chem.* **1993**, *32*, 4925−4934.

(54) Kojima, T.; Nakayama, K.; Ikemura, K.; Ogura, T.; Fukuzumi, S. Formation of a Ruthenium(IV)-Oxo Complex by Electron-Transfer

(55) Benet-Buchholz, J.; Comba, P.; Llobet, A.; Roeser, S.; Vadivelu, P.; Wadepohl, H.; Wiesner, S. Iron vs Ruthenium—A Comparison of the Stereoselectivity in Catalytic Olefin Epoxidation. *Dalton Trans.* **2009**, 5910−5923.

(56) Zong, R.; Naud, F.; Segal, C.; Burke, J.; Wu, F.; Thummel, R. Design and Study of Bi[1,8]naphthyridine Ligands as Potential Photooxidation Mediators in Ru(II) Polypyridyl Aquo Complexes. *Inorg. Chem.* **2004**, *43*, 6195−6202.

(57) Yang, X.-J.; Drepper, F.; Wu, B.; Sun, W.-H.; Haehnel, W.; Janiak, C. From Model Compounds to Protein Binding: Syntheses, Characterizations and Fluorescence Studies of [Ru^{II}(bipy)(terpy)L]$^{2+}$ Complexes (bipy = 2,2'-Bipyridine; terpy = 2,2':6',2"-Terpyridine; L = Imidazole, Pyrazole and Derivatives, Cytochrome *c*). *Dalton Trans.* **2005**, 256−267.

(58) Gupta, N.; Grover, N.; Neyhart, G. A.; Liang, W.; Singh, P.; Thorp, H. H. [RuO(dppz)(tpy)]$^{2+}$: a DNA Cleavage Agent with High DNA Affinity. *Angew. Chem., Int. Ed. Engl.* **1992**, *31*, 1048−1050.

(59) Staehle, R.; Tong, L.; Wang, L.; Duan, L.; Fischer, A.; Ahlquist, M. S. G.; Sun, L.; Rau, S. Water Oxidation Catalyzed by Mononuclear Ruthenium Complexes with a 2,2'-Bipyridine-6,6'-dicarboxylate (bda) Ligand: How Ligand Environment Influences the Catalytic Behavior. *Inorg. Chem.* **2014**, *53*, 1307−1319.

(60) Bernhard, P.; Bürgi, H.-B.; Hauser, H.; Lehmann, H.; Ludi, A. Syntheses and Crystal and Molecular Structures of Hexaaquaruthenium(II) *p*-Toluenesulfonate and Hexaaquaruthenium(III) *p*-Toluene-sulfonate, [Ru(H$_2$O)$_6$]-(C$_7$H$_7$SO$_3$)$_2$ and [Ru(H$_2$O)$_6$(C$_7$H$_7$SO$_3$)$_3$· 3H$_2$O. *Inorg. Chem.* **1982**, *21*, 3936−3941.

(61) Souza, M. L.; Castellano, E. E.; Telser, J.; Franco, D. W. Secondary Coordination Sphere Effects in Ruthenium(III) Tetraammine Complexes: Role of the Coordinated Water Molecule. *Inorg. Chem.* **2015**, *54*, 2067−2080.

(62) Nagao, H.; Aoyagi, K.; Yukawa, Y.; Howell, F. S.; Mukaida, M.; Kakihana, H. Chemical Behavior of an Oxygen Ligand in the Reaction between Oxo Complex of Ru^{IV} and Alcohols to Give Both Hydroxo and Alkoxo Complexes of Ru^{III}. *Bull. Chem. Soc. Jpn.* **1987**, *60*, 3247−3254.

(63) Bocé, M.; Tassé, M.; Mallet-Ladeira, S.; Pillet, F.; Da Silva, C.; Vicendo, P.; Lacroix, P. G.; Malfant, I.; Rols, M.-P. Effect of *trans*(NO, OH)-[RuFT(Cl)(OH)NO](PF$_6$) Ruthenium Nitrosyl Complex on Methicillin-Resistant *Staphylococcus epidermidis*. *Sci. Rep.* **2019**, *9*, 4867.

(64) Polyansky, D. E.; Muckerman, J. T.; Rochford, J.; Zong, R.; Thummel, R. P.; Fujita, E. Water Oxidation by a Mononuclear Ruthenium Catalyst: Characterization of the Intermediates. *J. Am. Chem. Soc.* **2011**, *133*, 14649−14665.

(65) Badiei, Y. M.; Polyansky, D. E.; Muckerman, J. T.; Szalda, D. J.; Haberdar, R.; Zong, R.; Thummel, R. P.; Fujita, E. Water Oxidation with Mononuclear Ruthenium(II) Polypyridine Complexes Involving a Direct Ru^{IV}=O Pathway in Neutral and Alkaline Media. *Inorg. Chem.* **2013**, *52*, 8845−8850.

(66) Dhuri, S. N.; Cho, K.-B.; Lee, Y.-M.; Shin, S. Y.; Kim, J. H.; Mandal, D.; Shaik, S.; Nam, W. Interplay of Experiment and Theory in Elucidating Mechanisms of Oxidation Reactions by a Nonheme Ru^{IV}O Complex. *J. Am. Chem. Soc.* **2015**, *137*, 8623−8632.

(67) Kojima, T.; Nakayama, K.; Sakaguchi, M.; Ogura, T.; Ohkubo, K.; Fukuzumi, S. Photochemical Activation of Ruthenium(II)-Pyridylamine Complexes Having a Pyridine-*N*-Oxide Pendant toward Oxygenation of Organic Substrates. *J. Am. Chem. Soc.* **2011**, *133*, 17901−17911.

(68) Ertem, M. Z.; Concepcion, J. J. Oxygen Atom Transfer as an Alternative Pathway for Oxygen−Oxygen Bond Formation. *Inorg. Chem.* **2020**, *59*, 5966−5974.

(69) Sousa, S. F.; Ertem, M. Z.; Faustino, L. A.; Machado, A. E. H.; Concepcion, J. J.; Maia, P. I. S.; Patrocinio, A. O. T. Mechanistic Investigation of the Aerobic Oxidation of 2-Pyridylacetate Coordi-

Oxidation of a Coordinatively Saturated Ruthenium(II) Complex and Detection of Oxygen-Rebound Intermediates in C-H Bond Oxygenation. *J. Am. Chem. Soc.* **2011**, *133*, 11692−11700.

nated to a Ru(II) Polypyridyl Complex. *Dalton Trans.* **2021**, *50*, 15248−15259.

(70) Moonshiram, D.; Pineda-Galvan, Y.; Erdman, D.; Palenik, M.; Zong, R.; Thummel, R.; Pushkar, Y. Uncovering the Role of Oxygen Atom Transfer in Ru-Based Catalytic Water Oxidation. *J. Am. Chem. Soc.* **2016**, *138*, 15605−15616.

(71) In this reaction, the methyl group of MP should be oxidatively lost to afford such as formaldehyde; however, those products were not observed in the ^{1}H NMR spectrum and could not be detected by Nash's method, since the absorption band derived from the Nash's reagent should overlap with those of **2** and **3**.

(72) The redox potential of the Ru[IV]/Ru[III] couple for **5** at pH = 1.0 was estimated from the Pourbaix diagram shown in Figure S10b, since the wave could not be observed due to the limit of the potential window for the experimental setup and complex **5** should exhibit dispoportionation to **2** and **6** at pH = 1.0.

(73) Morimoto, Y.; Park, J.; Suenobu, T.; Lee, Y.-M.; Nam, W.; Fukuzumi, S. Mechanistic Borderline of One-Step Hydrogen Atom Transfer versus Stepwise Sc[3+]-Coupled Electron Transfer from Benzyl Alcohol Derivatives to a Non-Heme Iron(IV)-Oxo Complex. *Inorg. Chem.* **2012**, *51*, 10025−10036.

(74) Park, J.; Morimoto, Y.; Lee, Y.-M.; Nam, W.; Fukuzumi, S. Unified View of Oxidative C-H Bond Cleavage and Sulfoxidation by a Nonheme Iron(IV)-Oxo Complex via Lewis Acid-Promoted Electron Transfer. *Inorg. Chem.* **2014**, *53*, 3618−3628.

(75) Ohzu, S.; Ishizuka, T.; Kotani, H.; Kojima, T. Reactivity of a Ru(III)-Hydroxo Complex in Substrate Oxidation in Water. *Chem. Commun.* **2014**, *50*, 15018−15021.

(76) To argue the HAT process, oxidation of cyclobutanol by **6** was examined under the same conditions. ^{1}H NMR spectrum of the D_2O solution after oxidation of cyclobutanol by **6** exhibited a complicated mixture of the oxidized products including ring-opening products as main products (Figure S24). This indicates that complex **6** undergoes HAT from cyclobutanol to afford the corresponding radical species.

(77) Kang, Y.; Chen, H.; Jeong, Y. J.; Lai, W.; Bae, E. H.; Shaik, S.; Nam, W. Enhanced Reactivities of Iron(IV)-Oxo Porphyrin **π**-Cation Radicals in Oxygenation Reactions by Electron-Donating Axial Ligands. *Chem.—Eur. J.* **2009**, *15*, 10039−10046.

(78) Liu, C.-J.; Yu, W.-Y.; Che, C.-M.; Yeung, C.-H. A Mechanistic Investigation of Alkene Epoxidation by Sterically Encumbered trans-Dioxoruthenium(VI) Porphyrins. *J. Org. Chem.* **1999**, *64*, 7365−7374.

(79) Park, J.; Lee, Y.-M.; Ohkubo, K.; Nam, W.; Fukuzumi, S. Efficient Epoxidation of Styrene Derivatives by a Nonheme Iron(IV)-Oxo Complex via Proton-Coupled Electron Transfer with Triflic Acid. *Inorg. Chem.* **2015**, *54*, 5806−5812.

(80) Lee, Y.-M.; Kim, S.; Ohkubo, K.; Kim, K.-H.; Nam, W.; Fukuzumi, S. Unified Mechanism of Oxygen Atom Transfer and Hydrogen Atom Transfer Reactions with a Triflic Acid-Bound Nonheme Manganese(IV)-Oxo Complex via Outer-Sphere Electron Transfer. *J. Am. Chem. Soc.* **2019**, *141*, 2614−2622.